

The evolution of the internal structure of massive star forming regions in the Milky Way as revealed by ALMA

Sami Dib¹

Max Planck Institute for Astronomy, Königstuhl 17, 69117, Heidelberg, Germany
e-mail: sami.dib@gmail.com; dib@mpia.de

September 28, 2022

ABSTRACT

We analyze the structure of 15 protocluster forming regions in the Milky Way using their 1.3 mm continuum emission maps from the ALMA-IMF large program. The analysis of the clouds structure is performed using the delta-variance spectrum technique. The calculated spectra display a self-similar regime on small scales as well as the presence of a prominent bump on larger scales and whose physical size, L_{hub} , falls in the range of ≈ 7000 au to 60000 au. These scales correspond to the sizes of the most compact clumps within the protocluster forming clouds. A significant correlation is found between L_{hub} and the surface density of the free-free emission estimated from the integrated flux of the H41 α recombination line ($\Sigma_{\text{H41}\alpha}^{\text{free-free}}$) as well as a significant anti-correlation between L_{hub} and the ratio of the 1.3 mm to 3 mm continuum emission fluxes ($S_{1.3\text{mm}}^{\text{cloud}}/S_{3\text{mm}}^{\text{cloud}}$). Smaller values of ($S_{1.3\text{mm}}^{\text{cloud}}/S_{3\text{mm}}^{\text{cloud}}$) and larger values of $\Sigma_{\text{H41}\alpha}^{\text{free-free}}$ correspond to more advanced evolutionary stages of the protocluster forming clumps. Hence, our results suggest that the sizes of the densest regions in the clouds are directly linked to their evolutionary stage and to their star formation activity with more evolved clouds having larger protocluster forming clumps. This is an indication that gravity plays a vital role in regulating the size and mass growth of these clumps with ongoing gas accretion.

Key words. stars: formation - ISM: clouds, general, structure, evolution - galaxies: ISM, star formation

1. Introduction

Massive stars play a vital role in the galactic ecosystem, both in the Milky Way and in external galaxies. Feedback from massive stars contributes a significant fraction of the galaxy's energy budget (Mac Low & Klessen 2004) and regulate the dynamics of interstellar gas on kpc scales down to smaller scales (≈ 10 pc) that are typical of the sizes of molecular clouds (Dib et al. 2006,2009; Bacchini et al. 2020; Lu et al. 2020; Ganguly et al. 2022). Massive stars are responsible for expelling the gas from star forming regions and for setting the star formation efficiency (Dib et al. 2011,2013; Hony et al. 2015; Kim et al. 2021). They are also the primary channel for the galactic chemical enrichment as they return their processed heavy elements into the galactic interstellar medium during their lifetimes in the form of stellar winds or at the time of their demise as supernova explosions (Izotov & Thuan 2000; Nomoto et al. 2013).

The formation of massive stars is a complex process that begins with the formation of their parental molecular clouds, the fragmentation of the clouds, and the formation of massive protostars (Zinnecker & Yorke 2007). The cloud assembly process can find its origin in generic thermal and gravitational instabilities (Dib & Burkert 2005) or by the collision of lower mass clouds (Dobashi et al. 2019; Fujita et al. 2021; Uchiyama et al. 2022). The fragmentation of massive clouds is regulated by competition between gravity and magnetic fields and the turbulent motions of the gas inherited from the cloud assembly phase as well as those generated by protostellar jets from the newly formed protostars (Cortes et al. 2008; Beuther et al. 2015,2019; Cunningham et al. 2018; Li et al. 2019; Liu et al. 2020; Liu et al. 2022; Beltrán et al. 2022). As massive stars evolve quickly towards the main

sequence, their strong radiation fields and stellar winds further impact the cloud structure and dynamical state (Carlsten & Hartigan 2018; Nayak et al. 2021; Rebollo et al. 2020; Tiwari et al. 2021).

In terms of global structure, massive star forming regions are often observed to have a hub-filament system architecture (e.g., Dib et al. 2020; Dewangan 2022; Zhou et al. 2022) with most, if not all protostars residing in the hub substructure (Kumar et al. 2020). In analyzing the global morphology of massive star forming regions and particularly of hub+filament systems, it is customary, and often very useful, to decompose the entire structure into a hub and a series of individual filaments in order to study both their individual and statistical properties (Kumar et al. 2020). A complementary approach in which the structure of the star-forming region as a whole is quantified can help shed light on how the total emission is distributed across different physical scales. In this work, we perform such an analysis on 15 massive star-forming regions in the Milky Way using the 1.3 mm continuum emission maps from the ALMA-IMF project. We quantify the internal structure of these star-forming regions using the delta-variance (Δ -variance) spectrum technique and we explore if and how features in the spectra relate to the clouds' evolutionary stages. The data is presented in Sect. 2 and the calculation of the Δ -variance is briefly summarized in Sect. 3. The results and conclusions are presented in Sect. 4 and Sect. 5, respectively.

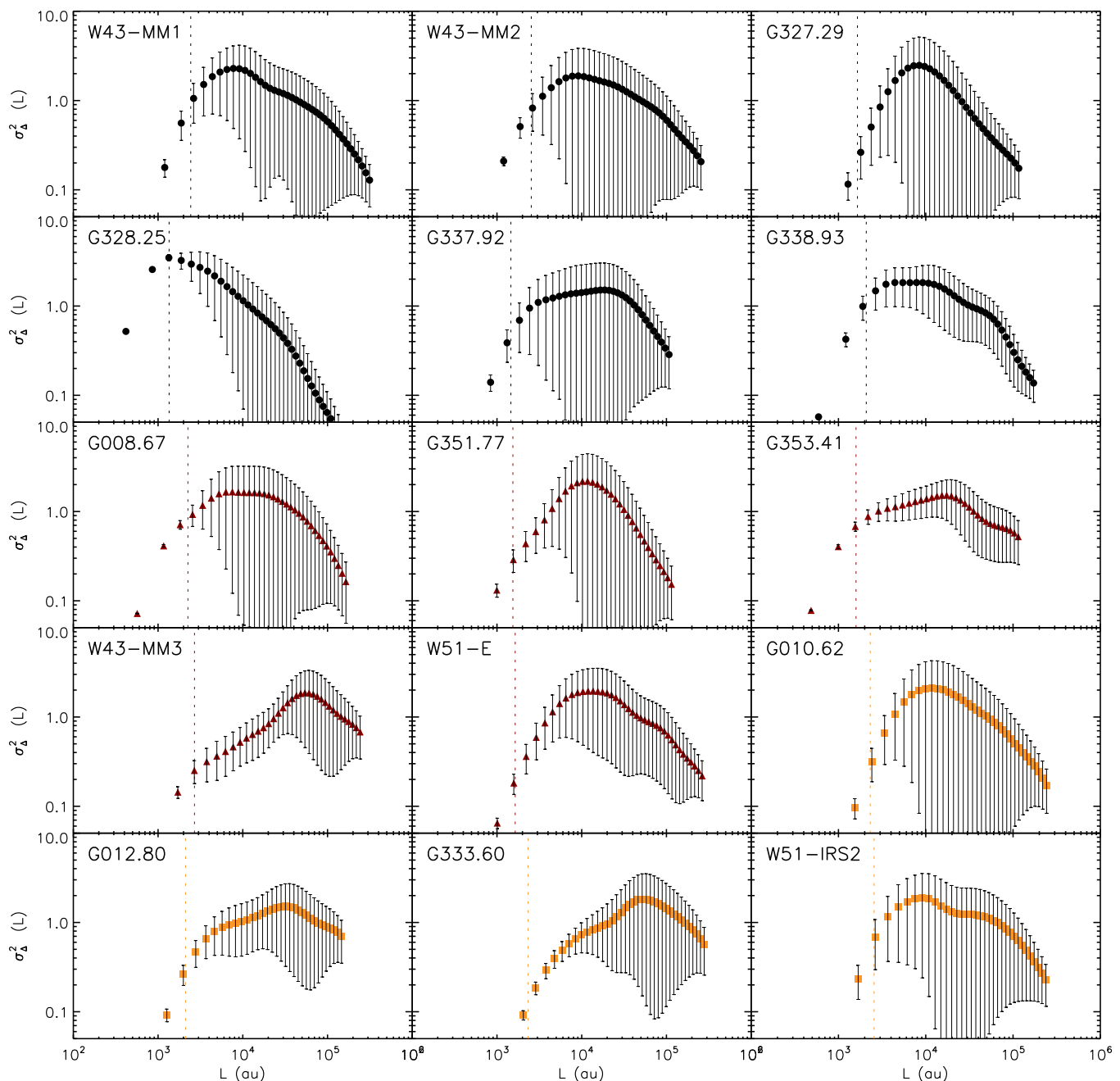


Fig. 1. The Δ -variance spectra of the 15 star forming regions in the ALMA-IMF sample. The spectra in black correspond to regions classified as Young, those in turquoise to those classified as Intermediate, and ones in yellow to those classified as Evolved (see text for details). The vertical dashed lines corresponds to the spatial resolution of the beam.

2. Data

We used data from the ALMA-IMF¹ project which is a large program of the *Atacama Large Millimeter Array* (ALMA) (Motte et al. 2022; Ginsburg et al. 2022). The sample consists of 15 massive star forming regions located at distances between ≈ 2 kpc to 5.5 kpc and that are in different evolutionary stages. Out of the 15 protocluster regions, six are categorized as being Young (Y), five as Intermediate (I), and four as Evolved (E). This classification in terms of evolutionary stage is based on two criteria which are the 1.3 mm to 3 mm flux ratio and the free-free emission at the H41 α frequency of the recombination line. The adoption

of these criteria is based on the assumption that as massive star forming regions evolve, they will host, statistically, an increasing number of H II regions. As these H II regions expand, their free-free emission increases. Furthermore, for evolved clouds, the free-free emission dominates at 3 mm, whereas emission at the 1.3 mm emission is dominated by thermal dust emission. This leads to ratios of the 1.3 mm to 3 mm emission that decrease as clouds evolve. Motte et al. measured the ratio of the 1.3 mm and 3 mm using the surface area of the 1.3 mm emission for each cloud ($S_{1.3\text{mm}}^{\text{cloud}}/S_{3\text{mm}}^{\text{cloud}}$) and they also made an estimate of the surface density of the free-free emission ($\Sigma_{\text{H41}\alpha}^{\text{free-free}}$). Ta-

¹ <https://www.almaimf.com/data.html>

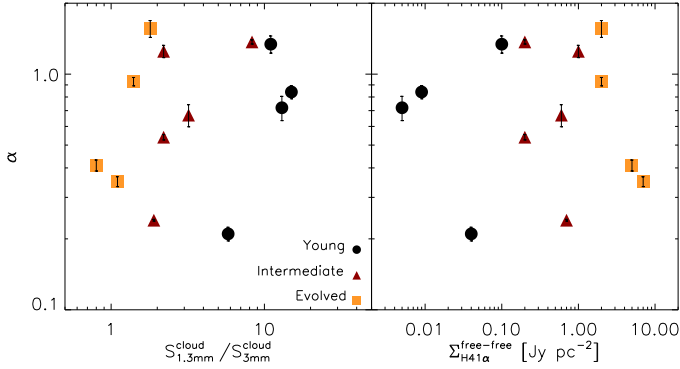


Fig. 2. Scatter plot between the slope of the Δ -variance spectrum in the self-similar regime, α , and the ratio ($S_{1.3\text{mm}}^{\text{cloud}}/S_{3\text{mm}}^{\text{cloud}}$) (left sub-panel) and between α and the surface density of the H41 α free-free emission (right sub-panel). The black circles are regions classified as Young, the dark red triangles correspond to those classified as Intermediate, and the yellow squares to those classified as evolved.

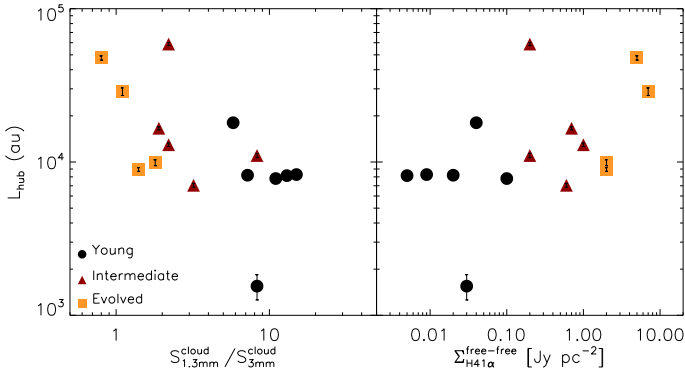


Fig. 3. Scatter plot between the peak found of the Δ -variance spectrum, L_{hub} , and the ratio ($S_{1.3\text{mm}}^{\text{cloud}}/S_{3\text{mm}}^{\text{cloud}}$) (left sub-panel) and between α and the surface density of the H41 α free-free emission (right sub-panel). The black circles are regions classified as Young, the dark red triangles correspond to those classified as Intermediate, and the yellow squares to those classified as evolved.

Table 1 lists the values of ($S_{1.3\text{mm}}^{\text{cloud}}/S_{3\text{mm}}^{\text{cloud}}$) and $\Sigma_{\text{H41}\alpha}^{\text{free-free}}$ measured by Motte et al. (2022).

For each protocluster, the current data products available from ALMA-IMF are two versions of a 1.3 mm and a 3 mm continuum maps which were obtained using the 12 m array configuration of ALMA (Ginsburg et al. 2022). The first version (bsens) is more sensitive, but is affected by emission lines present in each selected bandwidth. The second type of maps (cleanest) are built using the line-free channels. In this work, we will focus the analysis on the cleanest 1.3 mm maps. For these maps, the spatial resolution varies from region to region and is in the range of 1350 to 2690 au (see Table 5 in Motte et al. 2022).

3. Analysis: The Δ -variance spectrum

We quantified the structure of the 1.3 mm maps using the Δ -variance spectrum technique. The method was introduced in Stutzki et al. (1998) and Zielinsky et al. (1999) and is a generalization of the Allan variance (Allan 1966). In this work, we used an improved implementation of the method presented in

Ossenkopf et al. (2008a)². For a two-dimensional field $A(x, y)$, the Δ -variance on a scale L is defined as being the variance of the convolution of A with a filter function \odot_L , such that

$$\sigma_{\Delta}^2(L) = \frac{1}{2\pi} \langle (A * \odot_L)^2 \rangle_{x,y}. \quad (1)$$

For the filter function, Ossenkopf et al. (2008a) use a Mexican hat function which we also adopt here. This is defined as

$$\odot_L(r) = \frac{4}{\pi L^2} e^{-\frac{r^2}{(L/2)^2}} - \frac{4}{\pi L^2 (\nu^2 - 1)} \left[e^{-\frac{r^2}{(\nu L/2)^2}} - e^{-\frac{r^2}{(L/2)^2}} \right], \quad (2)$$

where the two terms on the right side of Eq. 2 represent the core and the annulus of the Mexican-hat function, respectively, and ν is the ratio of their diameters (we used a value of $\nu = 1.5$). For a faster and more efficient computation of Eq. 1 the calculation is performed as a multiplication in Fourier space (Ossenkopf et al. 2008a), and thus, the Δ -variance is given by

$$\sigma_{\Delta}^2(L) = \frac{1}{2\pi} \iint P |\bar{\odot}_L|^2 dk_x dk_y, \quad (3)$$

where P is the power spectrum of A , and $\bar{\odot}_L$ is the Fourier transform of the filter function. If β is the exponent of the power spectrum, then a relation exists between the slope of the Δ -variance and β (Stutzki et al. 1998). This is given by

$$\sigma_{\Delta}^2(L) \propto L^{\alpha} \propto L^{\beta-2}. \quad (4)$$

The slope of the Δ -variance can be measured from the range of spatial scales over which it displays a self-similar behavior. It can be related to the value of β . Characteristic scales are scales at which there are breaks of the self-similarity and that appear in the Δ -variance plots as break points or inflection points. The error bars of the Δ -variance are computed from the counting error determined by the finite number of statistically independent measurements in a filtered map and the variance of the variances, that is, the fourth moment of the filtered map. The Δ -variance has been used to analyze the structure of observed molecular clouds (Bensch et al. 2001; Sun et al. 2006; Ossenkopf et al. 2008b; Russeil et al. 2013; Dib et al. 2020; Schneider et al. 2022) as well the structure of the H I gas in nearby galaxies (Elmegreen et al. 2001; Dib et al. 2021). In molecular clouds, a variety of features can be observed in the Δ -variance spectrum (Dib et al. 2020; Schneider et al. 2022). Low surface-density clouds which are not forming stars display a self-similar regime which can be described by a single power law while at the other extreme, massive clouds that are intensely forming stars display features in their spectra which are associated with the existence of characteristic scales of the order of $\approx 0.8 - 1$ pc (Dib et al. 2020). Dib et al. (2020) interpreted this scale as representing the typical size of hubs in hub+filaments systems.

4. Results

Figure 1 displays the Δ -variance spectra of the 15 regions of the ALMA-IMF sample. The spectra are split into three sub-groups which represent the protocluster clouds classified as Young (black circles), Intermediate (dark red triangles), and Evolved (yellow squares) following the selection by Motte et al. (2022).

² <https://hera.ph1.uni-koeln.de/~ossk/Myself/deltavariance.htm>

Table 1. Inclinations and characteristics of the THINGS galaxy Δ -variance spectra.

Protocluster cloud name	$S_{1.3\text{mm}}^{\text{cloud}}/S_{3\text{mm}}^{\text{cloud}}$	$\Sigma_{\text{H}\alpha 41}^{\text{free-free}}$ [Jy pc $^{-2}$]	α	α -range [10^3 au]	L_{hub} [au]
W43-MM1	13	0.005	0.72	[3-6]	8150
W43-MM2	15	0.009	0.84	[3-6]	8280
G338.93	7.2	0.02	0.03	[3-10]	8200
G328.25	8.3	0.03	-	-	1550
G337.92	5.8	0.04	0.21	[3-10]	18040
G327.29	11	0.1	1.34	[3-6]	7800
G351.77	8.3	0.2	1.37	[3-6]	11025
G008.67	3.2	0.6	0.67	[3-6]	7050
W43-MM3	2.2	0.2	0.54	[3-10]	58800
W51-E	2.2	1	1.25	[3-6]	12960
G353.41	1.9	0.7	0.24	[3-15]	16600
G010.62	1.8	2	1.56	[3-6]	9900
W51-IRS2	1.4	2	0.93	[3-6]	8940
G012.80	1.1	7	0.35	[6-20]	28800
G333.60	0.8	5	0.41	[10-25]	47750

Notes. Columns represent the (1) name of protocluster cloud (2) the 1.3 mm to 3 mm flux ratio, measured on the area of the 1.3 mm emission, (3) the surface density of the free-free emission (4) the slope of the Δ -variance spectra in the self-similar regime (5) spatial range over which α is measured (6) position of the peak of the Δ -variance spectrum, L_{hub} .

The aim of this segregation is to verify whether the clouds' evolutionary stage has any connection to their internal structure. The first noticeable effect is that the spectra of all regions deviate from a single power law that is observed in low star forming regions (Dib et al. 2020; Yahia et al. 2021; Schneider et al. 2022). Instead, the Δ -variance spectra of the ALMA-IMF regions resemble those calculated for massive star forming regions found at lower distances and that have been obtained using data from the *Herschel* satellite such as NGC 6334, M17, and Cygnus X (Russeil et al. 2013; Dib et al. 2020; Schneider et al. 2022). The spectra are characterized by the presence of a bump on scales that range from several 10^3 au to several 10^4 au. These features are associated with the presence of over-dense structures that constitute the central hub(s) of the star forming clouds and such features are not observed in less massive regions, especially those that do not show signs of ongoing star formation (Dib et al. 2020). Figure 1 also shows that in regions that are classified as Evolved, the peaks of the spectra are present at larger physical scales than those found in less evolved regions.

We now explore the connection between features in the Δ -variance spectrum and the evolutionary criteria ($S_{1.3\text{mm}}^{\text{cloud}}/S_{3\text{mm}}^{\text{cloud}}$) and $\Sigma_{\text{H}\alpha 41}^{\text{free-free}}$. For each region, we extract two sets of information from the Δ -variance spectra. The first one is the slope of the spectra in the self-similar regime. As shown in Dib et al. (2020), the self-similar regime in the clouds could be perturbed by the presence of a bump and at the smallest scales, it can be affected by the effects of beam smearing which can extend beyond the actual beam size by a factor of ≈ 2 . We adopt a conservative approach and fit the spatial ranges of the spectra that display a clear self-similar regime, avoiding perturbed scales at both ends. The ranges over which a power law are fit to the self-similar regimes are listed in Tab. 1 along with the derived values of the exponent α . Figure 2 displays the values of α plotted against the ratio ($S_{1.3\text{mm}}^{\text{cloud}}/S_{3\text{mm}}^{\text{cloud}}$) (left sub-panel) and $\Sigma_{\text{H}\alpha 41}^{\text{free-free}}$ (right sub-panel). The G328.25 cloud is not included as its spectra does not show the presence of a self-similar regime on spatial scales below the peak. There are no correlation between α and ($S_{1.3\text{mm}}^{\text{cloud}}/S_{3\text{mm}}^{\text{cloud}}$)

(Spearman ρ coefficient of 0.16) and between α and $\Sigma_{\text{H}\alpha 41}^{\text{free-free}}$ (Spearman ρ coefficient of 0.10).

While the position of the peak, L_{hub} , can be estimated by eye, we derive a more accurate estimate of its value with a simple quadratic interpolation using several points around the peak. Figure 3 displays the value of L_{hub} plotted against the ($S_{1.3\text{mm}}^{\text{cloud}}/S_{3\text{mm}}^{\text{cloud}}$) ratio (left sub-panel) and $\Sigma_{\text{H}\alpha 41}^{\text{free-free}}$ (right sub-panel). A strong anti-correlation is clearly observed between the ($S_{1.3\text{mm}}^{\text{cloud}}/S_{3\text{mm}}^{\text{cloud}}$) ratio and L_{hub} (Spearman ρ coefficient of -0.62) and a strong correlation is observed between the latter and $\Sigma_{\text{H}\alpha 41}^{\text{free-free}}$ (Spearman ρ coefficient of 0.53).

The absence of any correlation between α with both the ($S_{1.3\text{mm}}^{\text{cloud}}/S_{3\text{mm}}^{\text{cloud}}$) ratio and $\Sigma_{\text{H}\alpha 41}^{\text{free-free}}$ is likely an indication that the self-similar structures that are observed in the 1.3 mm emission maps are not the result of turbulence cascading from larger scales into the clouds. On the other hand, the existence of a significant correlation between L_{hub} and ($S_{1.3\text{mm}}^{\text{cloud}}/S_{3\text{mm}}^{\text{cloud}}$) and of a significant anti-correlation between L_{hub} and $\Sigma_{\text{H}\alpha 41}^{\text{free-free}}$ clearly points to a significant role for gravity in driving the growth of the protocluster clump with continued gas accretion and in regulating turbulent motions in the clouds.

5. Conclusions

We calculated the Δ -variance spectra of all 15 protocluster forming clouds in the ALMA-IMF survey. The shapes of the spectra resemble those found earlier for closer massive star forming regions and all of them display a perturbed self-similar regime on small scales followed by a prominent bump at larger scales. This feature in the spectra is indicative of the presence of over-dense structures which are the region of ongoing and future massive star and cluster formation. The sizes of those regions, L_{hub} , is correlated with the surface density of the H41 α free-free emission and anti-correlated with the ratio of the 1.3 mm to 3 mm continuum emission fluxes ($S_{1.3\text{mm}}^{\text{cloud}}/S_{3\text{mm}}^{\text{cloud}}$). Since smaller values of ($S_{1.3\text{mm}}^{\text{cloud}}/S_{3\text{mm}}^{\text{cloud}}$) and larger values of $\Sigma_{\text{H}\alpha 41}^{\text{free-free}}$ correspond to

more advanced evolutionary stages of the protocluster forming clumps, this indicates that the size of the densest region in protocluster forming clouds is a direct indicator of its evolutionary stage, with larger clumps being associated with a more advanced evolutionary stage. We do not find any correlation between the value of the exponent of the power law that characterize the self-similar regime with either $\Sigma_{\text{H41}\alpha}^{\text{free-free}}$ or $(S_{1.3\text{mm}}^{\text{cloud}}/S_{3\text{mm}}^{\text{cloud}})$. These results indicate that turbulent motions which would set a self-similar regime in the clouds are not those inherited by a cascade from larger scales, but are mostly dominated by gravity-driven turbulence, with a potential contribution from feedback effects in the most evolves clouds. The correlation between L_{hub} and other evolutionary and star formation indicators is a clear indication that the densest regions of the clouds are dominated by gravity which must plays a major role in regulating their size and mass growth.

Acknowledgements. I thank Adam Ginsburg for very useful clarifications on aspects of the ALMA-IMF data and Volker Ossenkopf-Okada for helpful insight into the calculation of the Δ -variance spectra.

References

- Allan, D. 1966, *IEEEP*, 54, 221
 Bacchini, C. et al. 2020, *A&A*, 641, 70
 Beltrán, M. T., Rivilla, V. M., Cesaroni, R. et al. 2022, 659, 81
 Besch, F., Stutzki, J., Ossenkopf, V. 2001, *A&A*, 366, 636
 Beuther, H., Henning, T., Linz, H. et al. 2015, *A&A*, 581, 119
 Beuther, H., Ahmadi, A., Mottram, J. C. et al. 2019, *A&A*, 621, 122
 Carlsten, S. G., Hartigan, P. M. 2018, *ApJ*, 869, 77
 Cortes, P. C., Crutcher, R. M., Shepherd, D. S. et al. 2008, 676, 464
 Cunningham, N., Lumsden, S. L., Moore, T. J. T. et al. 2018, *MNRAS*, 477, 245
 Dewangan, L. K. 2022, *MNRAS*, 513, 294
 Dib, S., Burkert, A. 2005, *ApJ*, 630, 238
 Dib, S., Bell, E., Burkert, A. 2006, *ApJ*, 638, 797
 Dib, S., Walcher, C. J., Heyer, M. et al. 2009, *MNRAS*, 398, 1201
 Dib, S., Piau, L., Mohanty, S. et al. 2011, *MNRAS*, 415, 3439
 Dib, S., Gutkin, J., Brandner, W. et al. 2013, *MNRAS*, 436, 3727
 Dib, S., Henning, T. 2019, *A&A*, 629, 135
 Dib, S., Bontemps, S., Schneider, N. et al. 2020, *A&A*, 642, 177
 Dib, S. et al. 2021, *A&A*, 655, 101
 Dobashi, K., Shimoikura, T., Katakura, S. et al. 2019, *PASJ*, 71, 12
 Elmegreen, B. G., Kim, S., Staveley-Smith, L. 2001, *ApJ*, 548, 749
 Fujita, S., Sano, H., Enokiya R. et al. 2021, *PASJ*, 73, 172
 Ganguly, S. et al. 2022, *MNRAS*, arXiv:2204.02511
 Ginsburg, A., Csengeri, T., Galván-Madrid, R. et al. 2022, *A&A*, 662, 9
 Hony, S., Gouliermis, D. A., Galliano, F. et al. 2015, *MNRAS*, 448, 1847
 Izotov, Y. I., Thuan, T. X. 2000, *New Astron. Rev.*, 44, 329
 Kim, J.-G., Ostriker, E. C., Filippova, N. 2021, *ApJ*, 911, 128
 Kumar, M. S. N. et al. 2020, *A&A*, 642, 87
 Li, Q., Zhou, J., Esimbek, J. et al. 2019, *MNRAS*, 488, 463
 Liu, H.-J., Tej, A., Liu, T. et al. 2022, *MNRAS*, 511, 4480
 Liu, T., Evans, N. J., Kim, K.-T. et al. 2020, *MNRAS*, 496, 279
 Lu, Z.-J. et al. 2020, *ApJ*, 904, 58
 Mac Low, M.-M., Klessen, R. S. 2004, *RvMP*, 76, 125
 Motte, F., Bontemps, S., Csengeri, T. et al. 2022, *A&A*, 662, 8
 Nayak, O., Meixner, M., Okada, Y. et al. 2021, *ApJ*, 907, 106
 Nomoto, K., Kobayashi, C., Tominaga, N. 2013, *ARA&A*, 51, 457
 Ossenkopf, V., Krips, M., Stutzki, J. 2008a *A&A*, 485, 917
 Ossenkopf, V., Krips, M., Stutzki, J. 2008b *A&A*, 485, 719
 Rebolledo, D., Guzmán, A. E., Contreras, Y. et al. 2020, *ApJ*, 891, 113
 Russeil, D., Schneider, N., Anderson, L. D. et al. 2013, *A&A*, 554, 42
 Schneider, N. et al. 2022, *A&A*, arXiv:2207.14604
 Stutzki, J., Besch, F., Heithausen, A. et al. 1998, *A&A*, 336, 697
 Sun, K., Kramer, C., Ossenkopf, V. et al. 2006, *A&A*, 451, 539
 Tiwari, M., Menten, K. M., Wyrowski, F. et al. 2021, *A&A*, 644, 25
 Uchiyama, M. et al. 2022, *PASJ*, 73, 1638
 Yahia, H., Schneider, N., Bontemps, S. et al. 2021, *A&A*, 649, 33
 Zhou, J.-W., Liu, T., Evans, N. J. et al. 2022, *MNRAS*, 514, 603
 Zielinsky, M., Stutzki, J. 1999, *A&A*, 347, 630
 Zinnecker, H., Yorke, H. 2007, *ARA&A*, 45, 481